

Article

Assessing and Monitoring Forest Degradation in a Deciduous Tropical Forest in Mexico via Remote Sensing Indicators

Martin Enrique Romero-Sanchez ^{1,*}  and Raul Ponce-Hernandez ²

¹ National Institute for Forestry, Agriculture and Livestock Research, Progreso 5, Barrio de Santa Catarina, Coyoacan, Ciudad de Mexico 04010, Mexico

² School of the Environment, Trent University, Peterborough, ON K9J 7B8, Canada; rponce@trentu.ca

* Correspondence: romero.martin@inifap.gob.mx; Tel.: +52-553-626-8698

Received: 19 May 2017; Accepted: 11 August 2017; Published: 24 August 2017

Abstract: Assessing and monitoring forest degradation under national Monitoring, Verification and Reporting (MRV) systems in developing countries have been difficult to implement due to the lack of adequate technical and operational capacities. This study aims at providing methodological options for monitoring forest degradation in developing countries by using freely available remote sensing, forest inventory and ancillary data. We propose using Canopy Cover to separate, through a time series analysis approach using Landsat Imagery, forest areas with changes over time from sectors that report a “stable condition”. Above ground Biomass and Net Primary Productivity derived from remote sensing data were used to define thresholds for areas considered degraded. The approach was tested in a semi-deciduous tropical forest in the Southeast of Mexico. The results showed that higher rates of forest degradation, 1596 to 2865 ha year⁻¹, occur in areas with high population densities. The results also showed that 43% of the forests of the study area remain with no evident signs of degradation, as determined by the indicators used. The approach and procedures followed allowed for the identification and mapping of the temporal and spatial distribution of forest degradation, based on the indicators selected, and they are expected to serve as the basis for operations of the Reduction of Emissions from Deforestation and Forest Degradation (REDD+) initiative in Mexico and other developing countries, provided appropriate adaptations of the methodology are made to the conditions of the area in turn.

Keywords: REDD+; Landsat; forest modelling; forest degradation; Canopy Cover; Above-ground Biomass; Net Primary Productivity

1. Introduction

Reducing emissions from deforestation and forest degradation (REDD+) implies the implementation of efficient monitoring methods for providing high-quality data on forest degradation and its changes, according to reporting standards and IPCC guidelines [1]. Since its beginnings, one of the main criticisms of REDD+ has been that its measuring, reporting and verification (MRV) systems focus mainly on deforestation because it is easier to measure, as compared to forest degradation [2]. The main issue and obstacle in attaining and implementing a strong MRV system are sometimes the lack of reliable data, over time, for some forest types and, therefore, the substantial uncertainty involved in the estimates [3].

Methods for monitoring the current state and changes of forest carbon stocks within a REDD+ regime exploit the advantages and the potential of satellite-borne or airborne remote sensing imagery [4]. There are a fair number of studies that explore the capabilities of remote sensing in carbon accounting techniques under REDD+ strategies using different remote sensing approaches

and data to achieve the assessment [5–9]. One of the main advantages of using remote sensing data and procedures is that these have the potential to be decidedly instrumental in the assessment of forest degradation and deforestation processes at a much lower costs than any other methods [10,11]. However, the reality of REDD+ projects is that the methods for MRV used and implemented are unique to each location and strongly depend on how forest degradation (i.e., its definition) is understood and applied practically [12]. Moreover, it is essential that the components of forest degradation are clearly identified and amenable to accurate measurement, together with understanding how these are used against country requirements [13].

Direct detection of forest degradation processes relates area changes to and focuses on forest canopy damage [14]. These changes in forest attributes occurring during a period of time can be detected using information from forest resources inventories (FRI) and some from remote sensing [5,15]. Medium spatial resolution satellite remote sensing data such as Landsat Thematic Mapper (TM) and Enhanced Thematic Mapper plus (ETM+) have proven capable of obtaining regional-scale forest variables [16]. Their main advantage over higher resolution imagery resides on their being freely available as archival data for a relatively long time, thus providing a long-term time series [17]. This makes these images a suitable data source in developing countries, where costs are usually the main concern. However, it must be borne in mind that there are some limitations in estimating biomass implicit in the phenomenon of saturation for biomass due to the inability of incident and reflected energy to penetrate the canopy. These limitations have to be considered while using optical remote data [18]. Indirect approaches to forest degradation assessment usually focus on its spatial distribution relative to proximity to human infrastructure and the effects that the latter has on the degradation of forests nearby. Often, these “indirect” factors are used as “proxies” for the assessment of newly degraded areas [19].

Considering the absence of a universal or standard methodology for REDD+ that may be adapted to the conditions of a specific developing country, the present study attempts to develop a methodological framework that supports the assessment and monitoring of forest degradation to be implemented as part of a national REDD+ strategy.

The objective of this study is to implement an operational definition of what is understood by “forest degradation” and to identify measure and quantify its different degrees of intensity and its spatial extent in each landscape. The area selected for demonstrating the results of applying this methodological framework was the central region of the Yucatan Peninsula in Mexico, where the landscape is dominated by semi-deciduous tropical forests and a shifting slash-and-burn agriculture (SABA) land-use, which has been practised for centuries in these forests. This study shows the results from an empirical evaluation of its applicability with data from this specific region of Mexico. At the core of this methodology is the use of free satellite imagery (e.g., Landsat imagery) as a primary source of information.

One of the fundamental premises underpinning the selection of forest degradation indicators is the knowledge that the accumulation of biomass and carbon is related positively to the forest Net Primary Productivity (NPP) and thus, NPP is used to estimate the potential of the forest for storage of carbon under natural conditions [20]. Our main assumption relies on the principle that changes in NPP more accurately reflect forest condition, and therefore NPP is suitable to help in the definition of the reference state. This makes NPP a most suitable variable to be used as an indicator of forest degradation. Moreover, NPP together with aboveground biomass and canopy cover are variables used as main indicators of forest degradation [20].

Since canopy cover is a variable considered part of the definition of “forest” [21], including it as an indicator of forest degradation would allow for connecting and sharing definitions within and between countries, and in consequence, would enable the correspondence between thresholds of forest and no- forests among REDD+ participants. Forest canopy cover is recognized as a major biophysical and structural attribute of a forest because it affects terrestrial energy and water exchanges, photosynthesis and transpiration, net primary production, and carbon and nutrient fluxes [22]. Canopy cover provides

an attribute that is measurable and can be used to monitor and retrieve site-specific histories of different stages within the forest landscape dynamic [23]. Canopy Cover has already been used as an indicator to monitor and map forest degradation in different contexts [24,25].

As the avoidance of forest degradation (under the REDD+ strategy) seeks to maintain carbon in the living biomass on the ground, the most practical monitoring approach focuses on the assessment of Above-ground Biomass (AGB) as the main indicator of forest degradation. Assessment of AGB makes the monitoring of changes more targeted and efficient [14,26].

Although the design and implementation of a methodological framework for REDD+ presents many technical and practical challenges, the progress in the application of remote sensing science for forest assessments [9], together with the relatively recent changes in policies for access to remote sensing data [27,28] and the availability of consistent National Forest Inventory data converge in providing a valuable set of tools that yield valuable information is considered as the the basis for designing the methodology tested in our study.

2. Materials and Methods

2.1. Study Area

The area selected for this study lies in the central region of the Yucatan Peninsula in Mexico (Landsat World Reference System-2: Path 020, Row 046), inside of the watershed “Menda 1”, comprising nine sub-watersheds: “32-132-01-081”, “Bombahaltun”, “Emiliano Zapata”, “Labna”, “Sahcahmucuy”, “San Agustin”, “X-Kobenhaltun”, “Xul”, and “Yaxhachen” (Figure 1), where the landscape is dominated by semi-deciduous tropical forests punctuated by crop fields (maize, and other grains), and several rural settlements with various degrees of urbanisation. The agriculture in the area is strongly dominated by shifting cultivation, characterised by a slash-and-burn agriculture, mainly of a crop association of corn-beans-squash [29].

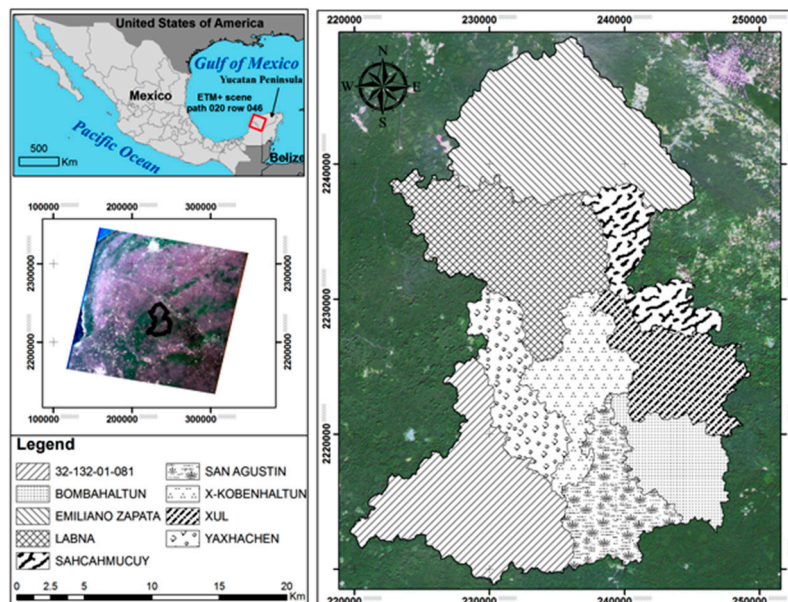


Figure 1. Study area “Menda 1” in the geographical context of the Yucatan Peninsula, Mexico.

2.2. Data

2.2.1. Landsat Imagery

Landsat Enhanced Thematic Mapper (ETM+) and Thematic Mapper (TM) imagery were obtained from the USGS website (<http://glovis.usgs.gov>). In the study area, as in other tropical regions, cloud

cover limited the choice of imagery available per year; however, the probability of acquiring at least one cloud-free Landsat image per season is relatively high [30]. In total, 155 Landsat scenes were downloaded. The images were in a L1T geometrically corrected format and were atmospherically corrected using the Second Simulation of a Satellite Signal in the Solar Spectrum (6S) radiative transfer approach [31].

Landsat 7 ETM+ images acquired with the SLC-off (i.e., SLC failure in 2003) were corrected using the Geostatistical Neighbour Spatial Pixel Interpolator algorithm, GNSPI, [32]. The GNSPI has proven to efficiently estimate pixels missing due to SLC failure, and its outputs are suitable for forest monitoring applications [33]. Landsat Images were separated according to their recording date (i.e., wet or dry season), and a first cloud filter was applied. Imagery with more than 10% cloud cover was avoided and was not included in the analysis.

2.2.2. High-Resolution Imagery

Available high spatial resolution images (provided by Google Earth™) were used to help in the interpretation of land cover classes and for the validation of the accuracy of the forest cover estimates. In addition, we used imagery from Google Earth for visual guidance in the interpretation of the trajectory analysis results.

2.2.3. Forest Inventory Sampling Plots

Sampling plots from the National Forestry and Soils Inventory databases (INFyS, National Forestry Commission, CONAFOR-Mexico) from periods 2004–2007 and 2009–2011 were used to estimate aboveground biomass at the watershed “Menda 1” scale. Each INFyS plot (1 ha) consists of four sub-plots (400 m²). These sub-plots are configured with a central sub-plot and three peripheral sub-plots located at 36.58 m and azimuths of 0, 135 and 225 from the central sub-plot. Dasometric databases from the National Forestry and Soils Inventory (INFyS) (2004–2007 and 2009–2011) were provided by the National Forestry Commission, Jalisco, Mexico (CONAFOR). A total of 149 sampling plots (72 from the period 2004–2007 and 77 from the period 2009–2011) distributed along the study area were used.

2.2.4. Meteorological and Ancillary Data

Meteorological data were acquired from the meteorological network of the National Institute of Forestry Agriculture and Livestock Research (INIFAP, Mexico City, Mexico) (<http://clima.inifap.gob.mx/redinifap/>) and the National Commission of Water (CONAGUA, Mexico City, Mexico) network. The INIFAP meteorological network collects an additional number of variables to those that are the standard meteorological network variables available. This data recording process started operations in 2007, and it is currently active. The climatic databases from INIFAP provided inputs for the NPP modelling process.

From the INIFAP meteorological network, five different meteorological stations were used in this study, distributed over the study area (Table 1). For each meteorological station, solar radiation (W/m²), daily mean, maximum and minimum temperature (°C), total precipitation (mm) and potential evapotranspiration (mm) were acquired from 1 January 2007 to 31 December 2013.

Digital elevation models (DEMs) and land use data, from the study area, were acquired from the National Institute of Statistics, Geography, and Informatics (INEGI, Aguascalientes, Mexico). The ArcGIS™ 10.3 software package was used to visualise, explore and process all spatial data of the study area extent. The spatial resolution of the data and the projection system were kept the same as the surface reflectance images.

Table 1. Meteorological stations used in this study.

Name	Location	Source	Coordinates (Lat., Long)
“Olochen”	Campeche	CONAGUA	20°00′13″ N, 89°44′1″ W
“Opelchen”	Campeche	CONAGUA	19°45′28″ N, 89°50′35″ W
“Xul”	Yucatan	CONAGUA	20°06′03″ N, 89°27′45″ W
“Tabi”	Yucatan	CONAGUA	20°13′39″ N, 89°31′55″ W
“Santa Elena”	Yucatan	CONAGUA	20°19′39″ N, 89°38′22″ W
“San Diego B.”	Yucatan	CONAGUA	19°51′22″ N, 089°17′52″ W
“Becanchen”	Yucatan	CONAGUA	20°00′13″ N, 89°44′1″ W
“Akil”	Yucatan	CONAGUA	20°14′39″ N, 089°19′29″ W
“Pozo 5”	Yucatan	INIFAP	20°21′53.4″ N, 89°28′39.3″ W
“El Chinal”	Yucatan	INIFAP	20°16′39.4″ N, 89°22′8.6″ W
“Inchek”	Campeche	INIFAP	19°44′13″ N, 89°57′59″ W
“Uxmal”	Yucatan	INIFAP	20°24′40.1″ N, 89°45′24.9″ W
“Parcela 28”	Yucatan	INIFAP	20°26′38.1″ N, 89°37′36.5″ W

2.3. Forest Degradation Concept

The first step in the methodological design required the identification of an operational definition of forest degradation and its component indicators. Two assumptions needed to be made to implement the trials with the methods: (a) that a comparison between an “optimal” and “non-optimal” state of the forest should be set to establish the reference state and (b) that the indicators selected reflect forest condition and help to define the reference state. Therefore, after conducting an intensive analysis of the literature, we based our definition of forest degradation mainly with reference to two approaches: the criterion/indicators [13] and the benchmark/landscape [12] methods.

The criterion/indicators approach uses five criteria that relate to drivers of degradation, loss of ecosystem services and the need for sustainable management, unusual disturbances, protected functions, and carbon storage. Then, a subset of at least seven indicators for the five criteria should be assessed to determine forest degradation [13]. The benchmark/landscape method uses a local benchmark that represents areas of low or no degradation that have comparable biophysical characteristics for measuring forest degradation [12].

In this approach, forest degradation is defined as the result of changes in forest structure that disrupt the capacity of a forest ecosystem to maintain carbon stocks under natural conditions. This definition is based on the use of a set of indicators, mainly derived from remote sensing data, and the establishment of a local benchmark (reference state), according to the criterion/indicators [13] and the benchmark/landscape [12] methods.

The set of indicators of forest degradation selected for this study were Forest Canopy Cover, Above-ground Biomass and Net Primary Productivity. These indicators were deliberately selected due to the ability to estimate their spatial and temporal variability under a remote sensing approach, using the time-series image stack. These indicators emerge from the definition of forest degradation provided above.

2.4. Estimation of Forest Degradation Indicators

2.4.1. Canopy Cover

The CLASlite™ image processing system [34] was used to develop the fractional cover and forest cover maps for the Landsat imagery dates over the study area. CLASlite™ can distinguish and separate Photosynthetic Vegetation (PV), Non-Photosynthetic Vegetation (NPV), and Bare Soil (S) into layers from the core process within CLASlite™ called “Automated Monte Carlo Unmixed Process” (AutoMCU). These outputs provide a quantitative analysis of the fractional or percentage cover (0–100%) of live and dead vegetation and bare substrate within each Landsat pixel [34]. The AutoMCU sub-model is based on a probabilistic algorithm designed for savanna, woodland, and shrubland

ecosystems and later modified for tropical forests [35,36]. The method uses three spectral endmember libraries to decompose each image pixel into three different elements that can be used to infer the percentage of forest canopy cover for each pixel of the Landsat imagery. The Photosynthetic Vegetation (PV) layer (0–100%) was used as an equivalent of field forest canopy cover (0–100%) for subsequent analysis.

Overall accuracy of the forest canopy cover layers was measured by computing the Kappa coefficient [37] from the percentage of pixels classified correctly in contingency tables, and by computing cross-tabulation quantities and allocation disagreement indices [38] against data from the field and forest inventory data.

2.4.2. Net Primary Productivity (NPP)

NPP was calculated according to the theory of Light Use Efficiency (LUE) as follows [39,40]:

$$\text{NPP} = \varepsilon \cdot \text{fPAR} \cdot \text{PAR} \quad (1)$$

where

PAR is photosynthetically active radiation (MJ/(m² month)),

fPAR is the fraction of PAR absorbed by vegetation canopy,

ε is the light use efficiency coefficient (g of C/MJ) and includes the plant respiration costs [41].

Light Use Efficiency Coefficient (ε)

The Light Use Efficiency coefficient ε was derived following the MODIS-GPP approach [42] where ε is calculated from two factors: the biome-specific maximum conversion efficiency ε_{max} and the effect of temperature $f(T)$ and water on plant photosynthesis $f(W)$ [39].

Estimation of fPAR and PAR

To estimate fPAR, an empirical relationship between fPAR as measured in the field, and the Normalized Difference Vegetation Index (NDVI), was used. Pearson correlation coefficients (r) were used to assess the strength of the relationship. NDVI was selected to correlate fPAR based on previous reports of successful correlation [40,43–45]. The measurements of fPAR (62) were taken randomly within the study area using a ceptometer model Accupar LP-80TM during the beginning of the rainy season of 2013. Due to the lack of available imagery that matches the period of the measurements, an image from 2012 within the rainy season (December) was used to derive the correlation coefficients. A linear model was fitted to derive values of fPAR from other satellite imagery.

Data acquired from meteorological stations as radiation (W/m²) were converted to PAR daily solar units (MJ). Then, solar radiation was converted to PAR using the coefficient 0.47 [40,46]. Later, daily PAR was converted to monthly values and spatially interpolated across the extent of the study area.

The Calculated Length Growing Period (LGP) [47] was used to separate and classify Landsat imagery to be used for monthly NPP estimates. LGP was used to avoid the mismatch of Landsat imagery within the wrong phenological state of the forest.

2.4.3. Above-Ground Biomass

Diameter at breast height (DBH), tree height (H) and species name were extracted from each sampling plot unit from the National Forest Inventory dataset and used for calculating individual tree above-ground biomass (AGB) for the species found in the study area. To estimate AGB per tree, we used allometric equations reported for the area [48]. These individual data (20,731 trees) were added on a per plot basis and used to extrapolate to a per hectare basis. Conversion of biomass/carbon from conglomerate to hectares was achieved using the “Ratio of Means” [49]. Later, AGB estimates were related to spectral variables obtained from satellite imagery.

Vegetation Indices

A review of a host of vegetation indices allowed for the identification of those that have been reported to estimate Above-ground Biomass accurately (Table 2). These indices were used to seek and identify those that are strongly correlated to forest biomass (AGB) measurements to generate estimates of biomass in the analysis. The calculation of the vegetation indices used reflectance values at different wavelengths so as to enhance information related to vegetation while reducing influences from environmental conditions and shade.

Table 2. Vegetation indices used in this study.

Vegetation Index	Equation	Author
Raw bands	G, R, NIR, MIR, SWIR	[50]
Normalized Difference Vegetation Index (NDVI)	$\frac{NIR - R}{NIR + R}$	[51]
Soil-Adjusted Vegetation Index (SAVI)	$\frac{(1 + L)(NIR - R)}{NIR + R + L}$	[52]
Normalized Difference Wetness Index (NDWI)	$\frac{NIR - MIR}{NIR + MIR}$	[53]
Enhanced Vegetation Index (EVI)	$2.5 \frac{(NIR - R)}{((NIR) + 6R - 7.5B + 1)}$	[54]
Green Vegetation Index (GVI)	$\frac{IR + SWIR}{R + MIR}$	[55]
NDVIc	$NDVI \cdot (1 - \frac{(MIR - MIR_{min})}{(MIR_{max} - MIR_{min})})$	[56]
Photosynthetic Vegetation (%) Layer (PV)	N/A	[57]

Above-Ground Biomass Estimation

Landsat Images from January 2005 and December 2010 were used as inputs to match the forest inventory data from periods 2004–2007 and 2009–2011, respectively. To estimate above-ground biomass, computed vegetation indices from Landsat imagery were resampled to a pixel size of 100 m to match the data from AGB plots at the same working scale (1 ha), for later analysis. The minimum and maximum values of the dataset were included in the calibration sample set selected, so that the domain limits of the model over which the validation process could be used, were included in the calibration. The remaining sampling points available were randomly divided into two groups consisting of 85% of the data points for model selection and 15% for validation.

Multiple regression analysis was used for biomass estimation. We evaluated the independent variables by using the variance influence factor (VIF) as multicollinearity normally occurs between remote sensed values [58]. To diminish multicollinearity problems, we applied a principal components analysis to generate new variables to develop biomass estimation models. The predictive models were validated using the leave-one-out cross-validation procedure by calculating the corresponding cross-validated coefficient of determination (R^2_{cv}) and the root mean square error ($RMSE_{cv}$).

A random sample representing the 15% of the field plots data was not included in the construction of the models but was used for validation purposes. We compared data extracted from the AGB estimates maps against data from the field and forest inventory databases by using the RMSE and RMSE%. In addition, we calculated the Pearson correlation coefficient (r) as a measure of linear fit between predictions and observations. All data analysis carried out in this study was performed using the “R” software package (<http://www.r-project.org/>).

2.5. Temporal Change Detection

To derive spatial and temporal patterns and to set up reference state for further comparisons, we conducted a multi-temporal analysis for selection of threshold values for the indicators used. We used

the BFAST and BFAST monitor algorithms [59,60] as the tools to perform a trajectory analysis of canopy cover derived from Landsat imagery (74) from the period 1987 to 2014. The Breaks For Additive Seasonal and Trend (BFAST) method is an iterative algorithm that combines the decomposition of time series into seasonal, trend, and remainder components as methods for detecting changes. BFAST integrates the iterative decomposition of time series into trend, seasonal and noise components with methods for detecting and characterizing changes within the time series [61].

The workflow to implement the BfastSpatial algorithm required the following steps: (a) pre-processing of surface reflectance data; (b) inventorying and preparing data for analysis and (c) analysis and formatting of change detection results. The algorithms were implemented using the BfastSpatial package for R software available at <http://github.com/dutri001/bfastSpatial>.

Change detection based on bi-temporal images [62] was implemented to detect Biomass and NPP change layers. The choice of this approach considered the fact that biomass/carbon data were available only in two different periods (2004–2007 and 2009–2011). Even though NPP data were available from the period 2007–2013, for the sake of completion, the bi-temporal change detection of this indicator was also computed.

2.6. Setting up a Reference State

First, the forest areas were isolated using the land cover map produced by the Mexican Government (INEGI, 2014), which was used later to compare it to the forest cover produced in this study. This step ensures consistency between outputs. Second, from the BFAST process, forest areas that show consistency (i.e., “stable” forests) from the time series analysis, were used to delineate the relative reference state (i.e., baseline) for forest areas. The next step followed was to calculate Net Primary Productivity and total carbon stocks for the areas highlighted with no change. Biomass (AGB) and NPP layers were used to compute Total Ecosystem Carbon Stock according to the carbon carrying capacity of the forest [20]. Values of AGB and NPP within areas with no change were used to set up reference states.

Field Validation

Visits to the study area during the beginning of the rainy season of 2013 were conducted to perform an independent collection of data (CC and AGB) and to validate some of the assumptions made during the initial stage of the research regardless of forest degradation. Using aid from local people, we were able to visit areas that are being used for agriculture, livestock and areas that had/have signals of selective logging, and areas with no evident signals of human intervention. Those areas were used as “ground truth” to verify partially the areas defined as part of the reference state and areas classified as degraded.

2.7. Forest Degradation Assessment

The final step in the analysis consisted of the integration of the indicators under a spatial context and their comparison against the references established before. The objective was to separate forest areas with changes over time from sectors that report a “stable condition” according to the methods described earlier. Next, the areas where changes were occurring were highlighted to provide information about the meaning of forest degradation (in terms of the indicator used) and the values associated with them (Mg/ha; gC/m²/year).

The methodological approach described here is shown in the flowchart in Figure 2.

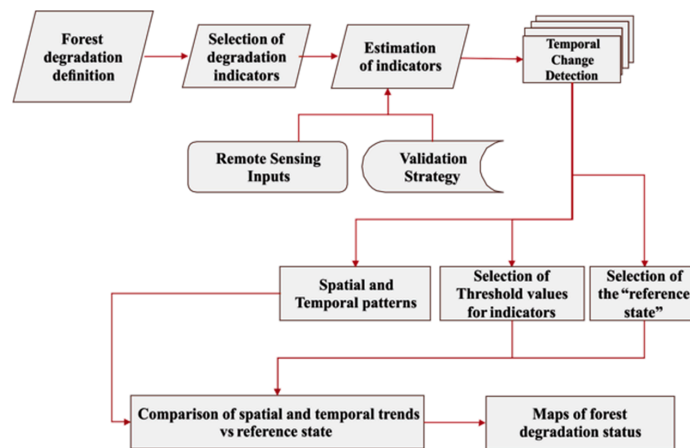


Figure 2. Methodological path to monitor and assess forest degradation in a dry semi-deciduous forest.

3. Results

3.1. Estimation of Forest Degradation Indicators

3.1.1. Canopy Cover

From the period 1990–2014, a total of 74 canopy cover layers were extracted from the fractional maps that CLASlite™ produced. The forest canopy cover layers (derived from the fractional cover map) were 90% correct (kappa coefficient) with zero and 10% of quantity and allocation disagreement, respectively, based on 1000 pixels assessed independently using available high-resolution imagery from Google Earth™.

3.1.2. Net Primary Productivity (NPP)

The Normalized Difference Vegetation Index (NDVI) was highly correlated ($r = 0.88$, $p < 0.05$) to fPAR, according to the Pearson correlation coefficient. Therefore, we fitted a linear equation ($a = -1.05$, $b = 2.45$, $R^2 = 0.76$) that estimates fPAR as a function of NDVI.

PAR (MJ/m^2) estimated from the meteorological station network (Figure 3) was used to derive NPP shown monthly. Its variability over time is shown in Figure 2. Given that Landsat imagery was not consistently acquired for all months of the years evaluated, where there was a lack of imagery, the closest Landsat imagery date to the required date was used to estimate NPP for a specific month. Therefore, we assumed that conditions of fPAR were similar on both dates.

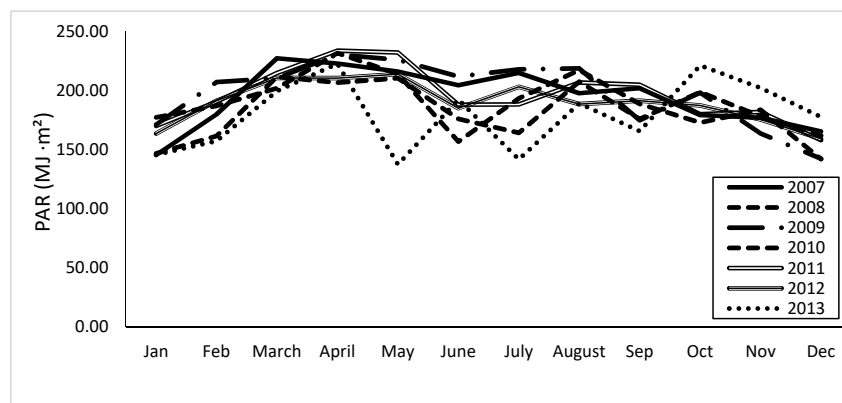


Figure 3. Temporal variation of average Photosynthetic Active Radiation (PAR) over the years in the study area.

NPP estimated from the period 2007–2013 showed a maximum value of 843 gC/m²/year and a mean of 547 gC/m²/year.

3.1.3. Above-ground Biomass (AGB)

From the vegetation indices tested, only those having significantly high correlation coefficients with biomass but having low correlation between each other were selected and used for biomass estimation (Table 3).

Table 3. Pearson correlation coefficients (*r*) from vegetation indices and Biomass (AGB).

	NDVI	IPVI	NDWI	EVI	TVI	SAVI	GVI	NDVIc	PV
AGB 04-07	0.74	0.74	0.73 *	0.64	0.73	0.74	0.73 *	0.75 *	0.74 *
AGB 09-11	0.73	0.73	0.76	0.65	0.73	0.73	0.87	0.76 *	0.68 *

* $p < 0.01$.

Above-ground Biomass showed a significant positive correlation ($\alpha = 0.01$) with most of the vegetation indices tested (Table 3). However, the Variance Influence Factor was above 50 for all independent variables. The Principal Component Analysis (PCA) created new variables and allowed the fitting of models for each one of the epochs, reducing the multicollinearity issue. The first and second principal components explained 99 percent of the total variance (Table 4).

Table 4. Principal components used for AGB estimations.

	PC1	PC2	Proportion of Variance
AGB 04-07	−0.998 (PV)	−0.991 (GVI)	0.99
AGB 09-011	−0.99 (PV)	−0.118 (NDWI)−0.978 (GVI)	0.99

The predictive models for estimating AGB were statistically significant ($p < 0.01$) (Table 5).

Table 5. Model selection for AGB estimation.

	Model *	R ²	R ² _{cv}
AGB 04-07	−22.3611−0.4228(PC1)−5.9179(PC2)	0.55	0.52
AGB 09-011	−49.0012−0.323(PC1)−19.01198(PC2)	0.48	0.46

* $p < 0.001$.

Estimations of AGB were within the range that previous reports have made for this type of vegetation. The uncertainties associated with the estimations are represented as the standard deviation of the mean and can be seen in Table 6.

Table 6. Aboveground biomass estimation summary.

AGB (Mg/ha)	Mean (SD *)	Max	Min
04-07	38.98 (10.11)	91.82	0.01
09-11	67.18 (31.03)	149.34	0.03

* Standard Deviation.

The error associated with the linear model for the period 04-07 (RMSE = 18.07 Mg/ha, RMSE% = 17%) obtained using the independent validation sample data was lower compared to the error presented by the 09-11 model (RMSE = 29.75 Mg/ha, RMSE% = 71.34%). Both models, 04-07 ($r = 0.75$) and 09-11 ($r = 0.74$), were successfully validated by comparing observed (15% of field data reserved for validation purposes) against estimated values.

3.2. Temporal Change Detection

The time series of imagery used here for canopy cover estimates had persistent and significant temporal gaps (as can be expected in a tropical forest [59]). The BFAST algorithm was able to identify trajectories where areas with “stable” forest cover and where degradation occurred. Table 7 presents the results of the BFAST monitor process applied to four pixels as an example and summarizes trajectories identified during the process.

Table 7. Example of Breakpoint detection using BFAST.

Pixel	Stable Period Selected (Year/DOY)	Monitoring Period Assessed (Years/DOY)	Break Detected (Year/DOY)	Model Fit (R ²)
A	1987 (267)–1999 (364)	2000 (1)–2014 (45)	2002 (204)	0.18
B	1995 (17)–1999 (364)	2000 (1)–2014 (45)	2002 (204)	0.53
C	1995 (17)–1999 (364)	2000 (1)–2014 (45)	2002 (204)	0.81
D	1987 (267)–1999 (364)	2000 (1)–2014 (45)	No Break detected	0.20

* DOY = Day of the year.

The trajectory analysis was able to identify and determine forest areas that maintained consistency in forest cover during the period of the analysis and those with changes over time (Figure 4).

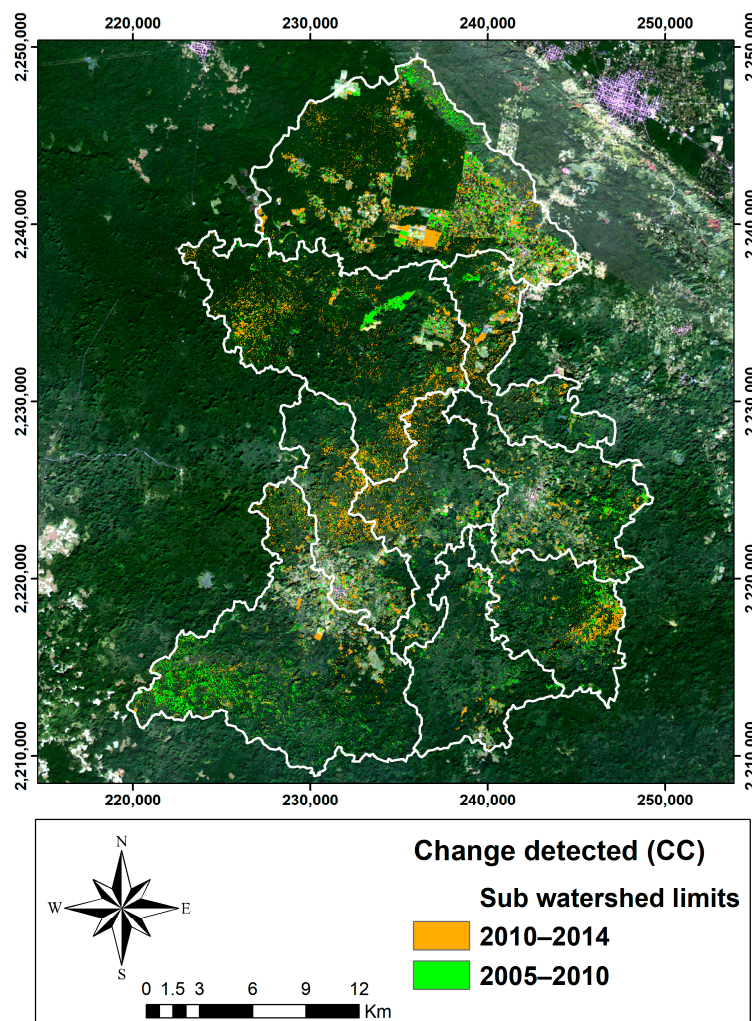


Figure 4. Areas identified as breakpoints for detection of forest degradation using Bfast.

Temporal change detection for NPP (2007, 2013) and the AGB (2004–2007; 2009–2011) performed by using an imaging differencing method captured decreases (degradation) in values of NPP and AGB on both dates compared.

3.3. Setting up a Reference State

To establish a benchmark for reference states, from the trajectory analysis (described earlier), we used the areas that maintained pixel observations above 80% of forest canopy cover as a base for the determination of “stable” forest cover. It has been assumed that the areas identified as “stable” are forest ecosystems that have reached maturity approaching an “equilibrium state”. For these areas, therefore, the carbon stocks are regarded as a reference of the maximum capacity of the forest to accumulate Carbon under similar conditions [63]. The forest that remains “stable” (i.e., with no significant change in canopy cover during the period evaluated) represents 43% (7444 ha) of the total surface of the watershed (Figure 5).

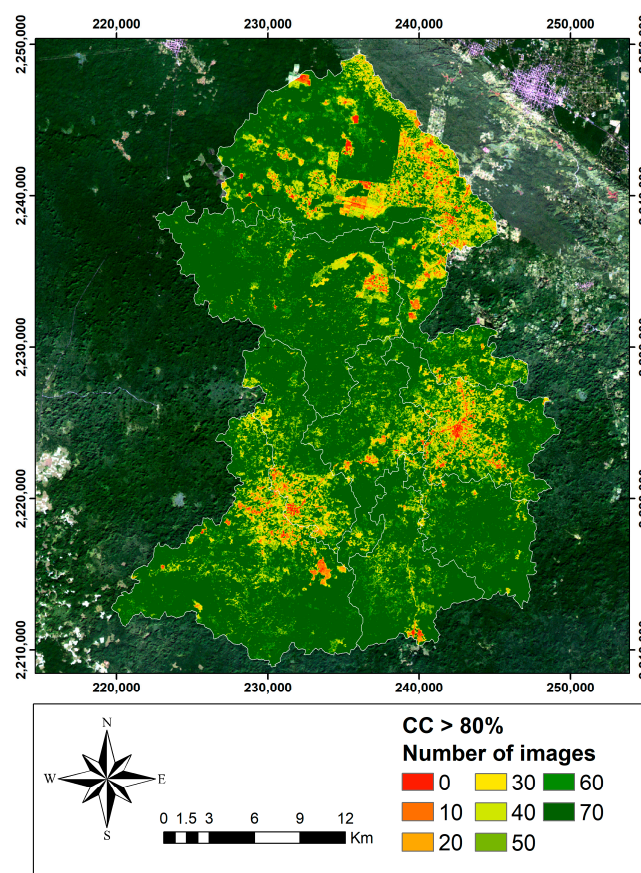


Figure 5. Observations where forest remains “stable”.

The “stable” forest cover layer identified was used to determine and delineate areas where the carbon capacity of the forest was set according to estimations of above-ground carbon density. Since the carbon capacity in this study was taken as equivalent to the total carbon in the ecosystem, the value that was reached as aboveground carbon was 51.84 Mg/ha, and the maximum rate of fixation of Carbon was estimated as 844 gC/m²/year (Table 8).

Table 8. Reference values for the study area.

	Carbon Mg/ha	NPP (gC/m ² /year)
min	14	205
Average	23.28	519
Max	51.84	844
St. Dev.	7.4	245

The integration of the different elements for the assessment and monitoring of forest degradation enabled the identification of areas that maintained a “stable” condition and areas that changed over the period evaluated. The latter are labelled as “forest degradation” areas (Figure 6).

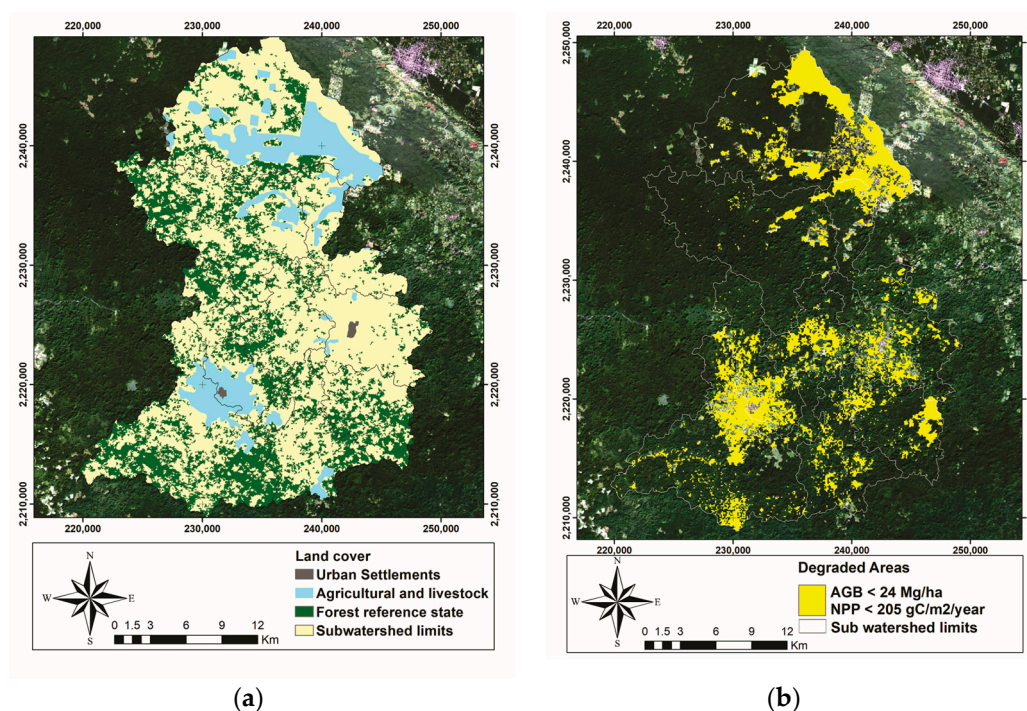


Figure 6. (a) Forest cover used as a reference state; (b) Forest-degraded areas according to the indicators selected.

The integration of the methods showed that the sub-watersheds in the study area with higher population density (“E. Zapata”, “31-132”, and “Xul”) have the upper rates of forest degradation (2865, 1611, and 1596 ha/year, respectively). Aboveground biomass estimations in forest areas identified as “not degraded” were in the range of 20 to 108 Mg·ha⁻¹; meanwhile, in “degraded” areas, the range classified as “degraded” ranged from 1 to 24 Mg ha⁻¹. The mean value of Net Primary Productivity for each one of the years evaluated was used as the threshold value for nondegraded areas. The areas classified with low NPP (<205 gC/m²/year) were located near urban settlements, which matches the results found earlier with Canopy cover (Figure 6).

4. Discussion and Conclusions

The approach followed in this study intends to support and complement national strategies for monitoring, verification and reporting of deforestation and forest degradation, especially in developing countries, where technical capacities and lack of data could be a major obstacle to monitoring changes in forest structure. This study showed that it is possible to produce, at minimum costs and with available data, maps with information about the status of forest cover and estimations of total carbon

stocks and productivity that ultimately can be used as tools for decision making concerning the volumes of Carbon involved, not only under the REDD+ strategy but also for national forest policies.

The spatial information produced by the methods proposed here, depending on their final use, would require adaptation and more processing, in order to be directly useful to other fields of enquiry, for example in biological applications. Thus far, information is only mapped at the pixel level (pixel resolution of 30 by 30 m) while most ecological users would prefer to work with patch-level phenomena. Moreover, the original maps typically include single-pixel noise (“speckle”) that is too small to either validate or interpret. Therefore, the next critical phase is one of spatial filtering, where adjacent pixels experiencing similar processes are grouped together into patches, and pixels in tiny patches are removed.

The results suggest that it is possible to produce clear canopy cover and biomass estimates at high resolution over relatively large areas. Since there are several options for the estimation of canopy cover, such as empirical modelling [64], regression trees [23] and spectral mixture analysis [65], this research adopted the spectral mixture analysis approach proposed by Asner et al., (2009) because it offers a standard procedure and has proven its applicability in the REDD+ context [66].

Concerning aboveground biomass, its estimation also turned out to be relatively accurate ($r = 0.74$, and $RMSE = 29$ Mg/ha), although problems with saturation above certain biomass values have been pointed out [67]. Some authors highlighted that including short wave infrared (SWIR) bands in the construction of AGB models may enhance sensitivity to the canopy water content and shadow fraction [68]. As a consequence, the capacity to predict AGB is improved. The best predictor models were precisely those that included vegetation indices based on calculations that included SWIR bands. It is important to notice that this type of approach can optimise resources used to obtain estimates of carbon with relative accuracy and a low cost, under the standards of MRV and REDD+. From estimations of AGB, it can be noted that low values of biomass correspond to areas that are very close to urban settlements and in consequence, are more prone to human disturbance and suffer some type of degradation [19]. It is important to note that the results from the estimations of AGB respond to the method used and the source of the data. From the Forest inventories that the National Forestry Commission provided, there are some inconsistencies in the data, and, as far as it can be possibly known, no quality control. In data from 2004–2007, quality control was undertaken; therefore, these data were deemed reliable. The results also showed the limitations that Vegetation indices could have in predicting biomass, due to problems of saturation.

The Net Primary Productivity of the forests also proved its value in identifying and mapping forest degradation. NPP is a forest parameter that is difficult to estimate empirically and can be subject to high levels of uncertainty [43,69,70]. The average values of Net Primary Productivity estimated from the years 2007–2013 in this study are closely comparable to those reported for similar ecosystems elsewhere [71,72]. It is possible to observe from that lower values of NPP were located near urban settlements and agricultural fields. This pattern of low NPP values near settlements and human activities suggests that the forests are being degraded (e.g., land cover modifications due to the dynamics of slash-and-burn agriculture) and that this degradation is related directly to human activities.

Although NPP estimations are difficult to perform and validate due to lack of field data, programs such the INIFAP’s meteorological network that register climatic variables every 15 min, and Eddy covariance towers networks, along with remote sensing data, are promissory elements to support NPP modelling in a reliable way in the Mexican context for the purposes of the REDD+ programme.

All human land activities that reduce the current carbon stock in a natural forest and therefore its natural carbon carrying capacity need to be included as the main driving forces and pressures on forest degradation, especially from a climate change perspective [73].

The determination of appropriate threshold values for classifying forest areas into forest degradation is crucial. The evidence has suggested that undisturbed forests can contribute significantly to the establishment of a benchmark that would enable the separation of “undegraded” and “degraded”

forest classes. In the case of AGB, previous studies indicate that higher values of AGB are likely to be encountered in undisturbed natural forests [12,63,74].

The procedures used in this study can be updated and implemented with satellite imagery of higher resolution (temporal and spatial), but this may require incurring significant costs. Organizations dedicated to the production of new remote sensing products and tools have developed new satellites sensors with higher spatial resolution, which represent a new age of terrestrial observation and digital mapping that can be applicable for the purposes of programs like REDD+ [75–79].

The improvements in spatial resolution (pixel size), spectral resolution (number of wavebands), radiometric resolution (sensitivity to detect radiation changes) and temporal resolution (data acquisition frequency), in optical remote sensing, bring the possibility of developing improved capabilities for measurement in quasi-real time [7,28,80,81]. These advances can be implemented at both, regional and national scales and may be used for national planning or REDD+ related monitoring verification systems, but also it is worth noting that the exploration of data fusion and the inclusion of active remote sensing data (e.g., Radar and LiDAR) as sources of information are promising research areas.

The decision to access the Landsat archive as the main source of satellite imagery was based on considerations of the availability and length of the historical archive and in the confirmed continuity of the program, at least until 2025 with Landsat 9 [17]. Moreover, Europe's Copernicus Earth Observation program includes the Sentinel-2 satellites designed to provide, under a free and open data policy, multiple global acquisitions with similar spectral and spatial characteristics as Landsat, ensuring continuity and a more robust archive to monitoring Earth's surface [28].

Within the REDD+ context, it is necessary to understand and identify the activities that are the drivers and pressures causing forest degradation. Further research on drivers and local activities is needed not only for formulating appropriate REDD+ strategies and policies but also for understanding the causal relationships at play in any given regional context. This would allow for the definition of suitable methods for measuring and monitoring drivers and local activities causing deforestation and forest degradation. The direct impact that climate change is having over physiological processes (e.g., productivity of tropical forests) and the spatial distribution of some species is also considered as future and a worthy avenue for enquiry and direction of research efforts.

Acknowledgments: This research was funded by the Mexican Council for Science and Technology (CONACyT) and the National Institute for Forestry, Agriculture and Livestock Research (INIFAP) of Mexico through a Ph.D. Thesis Research Grant awarded to the first author in the Environmental and Life Sciences Program at Trent University. The authors are deeply grateful for comments and suggestions during the review process, which were helpful in improving the manuscript.

Author Contributions: Martin Enrique Romero-Sanchez and Raul Ponce-Hernandez conceived and designed the research; Martin Enrique Romero-Sanchez performed and analysed the data. Raul Ponce-Hernandez provided methodological guidance. Both authors wrote and reviewed the paper.

Conflicts of Interest: The authors declare no conflict of interest.

References

1. Parker, C.; Mitchell, A.; Trivedi, M.; Mardas, N.; Sosis, K. *The Little REDD+ Book*; Global Canopy Programme: Oxford, UK, 2009.
2. Plugge, D.; Köhl, M. Estimating carbon emissions from forest degradation: Implications of uncertainties and area sizes for a REDD+ MRV system. *Can. J. For. Res.* **2012**, *42*, 1996–2010. [[CrossRef](#)]
3. Salimon, C.I.; Putz, F.E.; Menezes-Filho, L.; Anderson, A.; Silveira, M.; Brown, I.F.; Oliveira, L.C. Estimating state-wide biomass carbon stocks for a REDD plan in Acre, Brazil. *For. Ecol. Manag.* **2011**, *262*, 555–560. [[CrossRef](#)]
4. Global Observation of Forest and Land Cover Dynamics (GOFD-GOLD). *A Sourcebook of Methods and Procedures for Monitoring and Reporting Anthropogenic Greenhouse Gas Emissions and Removals Associated with Deforestation, Gains and Losses of Carbon Stocks in Forests Remaining Forests, and Forestation*; Land Cover Project Office, Wageningen University: Wageningen, The Netherlands, 2015.

5. Gibbs, H.K.; Brown, S.; Niles, J.O.; Foley, J.A. Monitoring and estimating tropical forest carbon stocks: Making REDD a reality. *Environ. Res. Lett.* **2007**, *2*, 45023. [[CrossRef](#)]
6. Olander, L.P.; Gibbs, H.K.; Steinger, M.; Swenson, J.J.; Murray, B.C. Reference scenarios for deforestation and forest degradation in support of REDD: A review of data and methods. *Environ. Res. Lett.* **2008**, *3*, 25011. [[CrossRef](#)]
7. Goetz, S.J.; Baccini, A.; Laporte, N.T.; Johns, T.; Walker, W.; Kellndorfer, J.; Houghton, R.A.; Sun, M. Mapping and monitoring carbon stocks with satellite observations: A comparison of methods. *Carbon Balance Manag.* **2009**, *4*, 2. [[CrossRef](#)] [[PubMed](#)]
8. Asner, G.P.; Powell, G.V.N.; Mascaró, J.; Knapp, D.E.; Clark, J.K.; Jacobson, J.; Kennedy-Bowdoin, T.; Balaji, A.; Paez-Acosta, G.; Victoria, E.; et al. High-resolution forest carbon stocks and emissions in the Amazon. *Proc. Natl. Acad. Sci. USA* **2010**, *107*, 16738–16742. [[CrossRef](#)] [[PubMed](#)]
9. Joseph, S.; Murthy, M.S.R.; Thomas, A.P. The progress on remote sensing technology in identifying tropical forest degradation: A synthesis of the present knowledge and future perspectives. *Environ. Earth Sci.* **2010**, *64*, 731–741. [[CrossRef](#)]
10. Mascaró, J.; Detto, M.; Asner, G.P.; Muller-Landau, H.C. Evaluating uncertainty in mapping forest carbon with airborne LiDAR. *Remote Sens. Environ.* **2011**, *115*, 3770–3774. [[CrossRef](#)]
11. Olander, L.P.; Galik, C.S.; Kissinger, G.A. Operationalizing REDD+: Scope of reduced emissions from deforestation and forest degradation. *Curr. Opin. Environ. Sustain.* **2012**, *4*, 661–669. [[CrossRef](#)]
12. Morales-Barquero, L.; Skutsch, M.; Jardel-Peláez, E.J.; Ghilardi, A.; Kleinn, C.; Healey, J.R. Operationalizing the definition of forest degradation for REDD+, with application to Mexico. *Forests* **2014**, *5*, 1653–1681. [[CrossRef](#)]
13. Thompson, I.D.; Guariguata, M.R.; Okabe, K.; Bahamondez, C.; Nasi, R.; Heymell, V.; Sabogal, C. An operational framework for defining and monitoring forest degradation. *Ecol. Soc.* **2013**, *18*, 20. [[CrossRef](#)]
14. Herold, M.; Román-Cuesta, R.M.; Mollicone, D.; Hirata, Y.; Van Laake, P.; Asner, G.P.; Souza, C.; Skutsch, M.; Avitabile, V.; Macdicken, K. Options for monitoring and estimating historical carbon emissions from forest degradation in the context of REDD+. *Carbon Balance Manag.* **2011**, *6*, 13. [[CrossRef](#)] [[PubMed](#)]
15. Global Forest Observations Initiative (GFOI). *Integrating Remote-Sensing and Ground-Based Observations for Estimation of Emissions and Removals of Greenhouse Gases in Forests: Methods and Guidance from Global Forest Observations Initiative*, 2014th ed.; Group on Earth Observations: Geneva, Switzerland, 2013.
16. Wulder, M.A.; Kurz, W.A.; Gillis, M. National level forest monitoring and modeling in Canada. *Prog. Plan.* **2004**, *61*, 365–381. [[CrossRef](#)]
17. Wulder, M.A.; Masek, J.G.; Cohen, W.B.; Loveland, T.R.; Woodcock, C.E. Opening the archive: How free data has enabled the science and monitoring promise of Landsat. *Remote Sens. Environ.* **2012**, *122*, 2–10. [[CrossRef](#)]
18. Sánchez-Azofeifa, G.A.; Castro-Esau, K.L.; Kurz, W.A.; Joyce, A. Monitoring carbon stocks in the tropics and the remote sensing operational limitations: From local to regional projects. *Ecol. Appl.* **2009**, *19*, 480–494. [[CrossRef](#)] [[PubMed](#)]
19. Moreno-Sanchez, R.; Torres-Rojo, J.M.; Moreno-Sanchez, F.; Hawkins, S.; Little, J.; McPartland, S. National assessment of the fragmentation, accessibility and anthropogenic pressure on the forests in Mexico. *J. For. Res.* **2012**, *23*, 529–541. [[CrossRef](#)]
20. Keith, H.; Mackey, B.; Berry, S.; Lindenmayer, D.; Gibbons, P. Estimating carbon carrying capacity in natural forest ecosystems across heterogeneous landscapes: Addressing sources of error. *Glob. Chang. Biol.* **2010**, *16*, 2971–2989. [[CrossRef](#)]
21. Food and Agriculture Organization (FAO). *Global Forest Resources Assessment*; Food and Agriculture Organization of the United Nations: Rome, Italy, 2010.
22. Nadkarni, N.M.; Parker, G.G.; Rinker, H.B.; Jarzen, D.M. The nature of forest canopies. In *Forest Canopies*; Lowman, M., Rinker, B., Eds.; Elsevier Inc.: Sarasota, FL, USA, 2004; Volume 54, p. 517.
23. Sexton, J.O.; Song, X.-P.; Feng, M.; Noojipady, P.; Anand, A.; Huang, C.; Kim, D.-H.; Collins, K.M.; Channan, S.; DiMiceli, C.; et al. Global, 30-m resolution continuous fields of tree cover: Landsat-based rescaling of MODIS vegetation continuous fields with lidar-based estimates of error. *Int. J. Digit. Earth* **2013**, *6*, 427–448. [[CrossRef](#)]
24. Panta, M.; Kim, K.; Joshi, C. Temporal mapping of deforestation and forest degradation in Nepal: Applications to forest conservation. *For. Ecol. Manag.* **2008**, *256*, 1587–1595. [[CrossRef](#)]

25. Mon, M.S.; Mizoue, N.; Htun, N.Z.; Kajisa, T.; Yoshida, S. Factors affecting deforestation and forest degradation in selectively logged production forest: A case study in Myanmar. *For. Ecol. Manag.* **2012**, *267*, 190–198. [[CrossRef](#)]
26. Köhl, M.; Baldauf, T.; Plugge, D.; Krug, J. Reduced emissions from deforestation and forest degradation (REDD): A climate change mitigation strategy on a critical track. *Carbon Balance Manag.* **2009**, *4*, 10. [[CrossRef](#)] [[PubMed](#)]
27. Woodcock, C.E.; Allen, R.; Anderson, M.; Belward, A.; Bindschadler, R.; Cohen, W.; Gao, F.; Goward, S.N.; Helder, D.; Helmer, E.; et al. Free access to Landsat imagery. *Science* **2008**, *320*, 1011. [[CrossRef](#)] [[PubMed](#)]
28. Roy, D.P.; Wulder, M.A.; Loveland, T.R.; Ilen, R.G.; Anderson, M.C.; Helder, D.; Irons, J.R.; Johnson, D.M.; Kennedy, R.; Scambos, T.A.; et al. Landsat-8: Science and product vision for terrestrial global change research. *Remote Sens. Environ.* **2014**, *145*, 154–172. [[CrossRef](#)]
29. Hernández-Stefanoni, J.L.; Dupuy, J.M.; Tun-Dzul, F.; May-Pat, F. Influence of landscape structure and stand age on species density and biomass of a tropical dry forest across spatial scales. *Landsc. Ecol.* **2010**, *26*, 355–370. [[CrossRef](#)]
30. Ju, J.; Roy, D.P. The availability of cloud-free Landsat ETM+ data over the conterminous United States and globally. *Remote Sens. Environ.* **2008**, *112*, 1196–1211. [[CrossRef](#)]
31. Masek, J.G.; Vermote, E.F.; Saleous, N.E.; Wolfe, R.; Hall, F.G.; Huemmrich, K.F.; Gao, F.; Kutler, J.; Lim, T.-K. A Landsat Surface Reflectance Dataset for North America, 1990–2000. *IEEE Geosci. Remote Sens. Lett.* **2006**, *3*, 68–72. [[CrossRef](#)]
32. Zhu, X.; Liu, D.; Chen, J. A new geostatistical approach for filling gaps in Landsat ETM+ SLC-off images. *Remote Sens. Environ.* **2012**, *124*, 49–60. [[CrossRef](#)]
33. Romero-Sanchez, M.E.; Ponce-Hernandez, R.; Franklin, S.E.; Aguirre-Salado, C.A. Comparison of data gap-filling methods for Landsat ETM+ SLC-off imagery for monitoring forest degradation in a semi-deciduous tropical forest in Mexico. *Int. J. Remote Sens.* **2015**, *36*, 2786–2799. [[CrossRef](#)]
34. Asner, G.P.; Knapp, D.E.; Balaji, A.; Paez-Acosta, G. Automated mapping of tropical deforestation and forest degradation: CLASlite. *J. Appl. Remote Sens.* **2009**, *3*, 33543. [[CrossRef](#)]
35. Asner, G.P.; Heidebrecht, K.B. Spectral Unmixing of Vegetation, Soil and Dry Carbon in Arid Regions: Comparing Multispectral and Hyperspectral Observations. *Int. J. Remote Sens.* **2002**, *23*, 3939–3958. [[CrossRef](#)]
36. Asner, G.P.; Keller, M.; Pereira, R.; Zweede, J.C.; Jose, N.; Silva, M. Canopy Damage and Recovery after Selective Logging in Amazonia: Field and Satellite Studies. *Ecol. Appl.* **2004**, *14*, 280–298. [[CrossRef](#)]
37. Congalton, R.; Kass, G. *Assessing the Accuracy of Remotely Sensed Data: Principles and Practices*, 2nd ed.; CRC Press, Taylor & Francis Group: Boca Raton, FL, USA, 2009.
38. Pontius, R.G.; Millones, M. Death to Kappa: Birth of quantity disagreement and allocation disagreement for accuracy assessment. *Int. J. Remote Sens.* **2011**, *32*, 4407–4429. [[CrossRef](#)]
39. Yuan, W.; Liu, S.; Zhou, G.; Zhou, G.; Tieszen, L.L.; Baldocchi, D.; Bernhofer, C.; Gholz, H.; Goldstein, A.H.; Goulden, M.L.; et al. Deriving a light use efficiency model from eddy covariance flux data for predicting daily gross primary production across biomes. *Agric. For. Meteorol.* **2007**, *143*, 189–207. [[CrossRef](#)]
40. Huang, N.; Niu, Z.; Wu, C.; Tappert, M.C. Modeling net primary production of a fast-growing forest using a light use efficiency model. *Ecol. Model.* **2010**, *221*, 2938–2948. [[CrossRef](#)]
41. Running, S.W.; Thornton, P.E.; Nemani, R.R.; Glassy, J.M. Global terrestrial gross and net primary productivity from the Earth Observing system. In *Methods in Ecosystem Science*; Sala, O.E., Jackson, R.B., Mooney, H.A., Howart, R.W., Eds.; Springer: New York, NY, USA, 2000; pp. 44–57.
42. Running, S.W.; Nemani, R.; Glassy, J.M.; Thornton, P.E. *Modis Daily Photosynthesis (Psn) and Annual Net Primary Production (Npp) Product*; Algorithm Theoretical Basis Document. Version 3; Oak Ridge National Laboratory: Oak Ridge, TN, USA, 1999.
43. Wang, L.; Gong, W.; Ma, Y.; Zhang, M. Modeling Regional Vegetation NPP Variations and Their Relationships with Climatic Parameters in Wuhan, China. *Earth Interact.* **2013**, *17*, 1–20. [[CrossRef](#)]
44. McCallum, I.; Wagner, W.; Schmulilius, C.; Shvidenko, A.; Obersteiner, M.; Fritz, S.; Nilsson, S. Satellite-based terrestrial production efficiency modeling. *Carbon Balance Manag.* **2009**, *4*, 8. [[CrossRef](#)] [[PubMed](#)]
45. Running, S.W.; Nemani, R.R.; Heinsch, F.A.; Zhao, M.; Reeves, M.; Hashimoto, H. A Continuous Satellite-Derived Measure of Global Terrestrial Primary Production. *Bioscience* **2004**, *54*, 547. [[CrossRef](#)]

46. Akmal, M.; Janssens, M.J.J. Productivity and light use efficiency of perennial ryegrass with contrasting water and nitrogen supplies. *Field Crop. Res.* **2004**, *88*, 143–155. [[CrossRef](#)]
47. Food and Agriculture Organization (FAO). *Report on the Agro-Ecological Zones Project*; World soil resource report 48; Food and Agriculture Organization of the United Nations: Rome, Italy, 1978.
48. Chave, J.; Réjou-Méchain, M.; Búrquez, A.; Chidumayo, E.; Colgan, M.S.; Delitti, W.B.C.; Duque, A.; Eid, T.; Fearnside, P.M.; Goodman, R.C.; et al. Improved allometric models to estimate the aboveground biomass of tropical trees. *Glob. Chang. Biol.* **2014**, *20*, 3177–3190. [[CrossRef](#)] [[PubMed](#)]
49. Šmelko, Š.; Merganič, J. Some methodological aspects of the National Forest Inventory and Monitoring in Slovakia. *J. For. Sci.* **2008**, *54*, 476–483.
50. Aguirre-Salado, C.A.; Treviño-Garza, E.J.; Aguirre-Calderón, O.A.; Jiménez-Pérez, J.; González-Tagle, M.A.; Valdez-Lazalde, J.R.; Miranda-Aragón, L.; Aguirre-Salado, A.I. Construction of aboveground biomass models with remote sensing technology in the intertropical zone in Mexico. *J. Geogr. Sci.* **2012**, *22*, 669–680. [[CrossRef](#)]
51. Rouse, J.W.J.; Hass, R.H.; Schell, J.A.; Deering, D.W. *Monitoring Vegetation Systems in the Great Plains with Ertis*; NASA Special Publication: Washington, DC, USA, 1974; pp. 309–317.
52. Huete, A. A soil-adjusted vegetation index (SAVI). *Remote Sens. Environ.* **1988**, *25*, 295–309. [[CrossRef](#)]
53. Hardisky, M.A.; Klemas, V.; Smart, R.M. The influence of soil salinity, growth form, and leaf moisture on the spectral radiance of spartina alterniflora canopies. *Photogramm. Eng. Remote Sens.* **1983**, *49*, 77–83.
54. Huete, A. A comparison of vegetation indices over a global set of TM images for EOS-MODIS. *Remote Sens. Environ.* **1997**, *59*, 440–451. [[CrossRef](#)]
55. Nageswara Rao, P.P.; Mohankumar, A. Cropland inventory in the command area of Krishnarajasagar project using satellite data. *Int. J. Remote Sens.* **1994**, *15*, 1295–1305. [[CrossRef](#)]
56. Nemani, R.; Pierce, L.; Running, S.; Band, L. Forest ecosystem processes at the watershed scale: Sensitivity to remotely-sensed Leaf Area Index estimates. *Int. J. Remote Sens.* **1993**, *14*, 2519–2534. [[CrossRef](#)]
57. Asner, G.P. Tropical forest carbon assessment: integrating satellite and airborne mapping approaches. *Environ. Res.* **2009**, *4*, 34009. [[CrossRef](#)]
58. Chen, Q.; Vaglio Laurin, G.; Battles, J.J.; Saah, D. Integration of airborne lidar and vegetation types derived from aerial photography for mapping aboveground live biomass. *Remote Sens. Environ.* **2012**, *121*, 108–117. [[CrossRef](#)]
59. DeVries, B.; Verbesselt, J.; Kooistra, L.; Herold, M. Robust monitoring of small-scale forest disturbances in a tropical montane forest using Landsat time series. *Remote Sens. Environ.* **2015**, *161*, 107–121. [[CrossRef](#)]
60. Verbesselt, J.; Zeileis, A.; Herold, M. Near real-time disturbance detection using satellite image time series. *Remote Sens. Environ.* **2012**, *123*, 98–108. [[CrossRef](#)]
61. Verbesselt, J.; Hyndman, R.; Newnham, G.; Culvenor, D. Detecting trend and seasonal changes in satellite image time series. *Remote Sens. Environ.* **2010**, *114*, 106–115. [[CrossRef](#)]
62. Hussain, M.; Chen, D.; Cheng, A.; Wei, H.; Stanley, D. Change detection from remotely sensed images: From pixel-based to object-based approaches. *ISPRS J. Photogramm. Remote Sens.* **2013**, *80*, 91–106. [[CrossRef](#)]
63. Yingchun, L.; Guirui, Y.; Qiufeng, W.; Yangjian, Z. Huge Carbon Sequestration Potential in Global Forests. *J. Resour. Ecol.* **2012**, *3*, 193–201. [[CrossRef](#)]
64. Carreiras, J.M.B.; Pereira, J.M.C.; Pereira, J.S. Estimation of tree canopy cover in evergreen oak woodlands using remote sensing. *For. Ecol. Manag.* **2006**, *223*, 45–53. [[CrossRef](#)]
65. Souza, C., Jr.; Siqueira, J.; Sales, M.; Fonseca, A.; Ribeiro, J.; Numata, I.; Cochrane, M.; Barber, C.; Roberts, D.; Barlow, J. Ten-Year Landsat Classification of Deforestation and Forest Degradation in the Brazilian Amazon. *Remote Sens.* **2013**, *5*, 5493–5513.
66. Reimer, F.; Asner, G.P.; Joseph, S. Advancing reference emission levels in subnational and national REDD+ initiatives: A CLASlite approach. *Carbon Balance Manag.* **2015**, *10*, 5. [[CrossRef](#)] [[PubMed](#)]
67. Zhu, X.; Liu, D. Improving forest aboveground biomass estimation using seasonal Landsat NDVI time-series. *ISPRS J. Photogramm. Remote Sens.* **2015**, *102*, 222–231. [[CrossRef](#)]
68. Avitabile, V.; Baccini, A.; Friedl, M.A.; Schmillius, C. Capabilities and limitations of Landsat and land cover data for aboveground woody biomass estimation of Uganda. *Remote Sens. Environ.* **2012**, *117*, 366–380. [[CrossRef](#)]
69. Prieto-Blanco, A.; North, P.R.J.; Barnsley, M.J.; Fox, N. Satellite-driven modelling of Net Primary Productivity (NPP): Theoretical analysis. *Remote Sens. Environ.* **2009**, *113*, 137–147. [[CrossRef](#)]

70. Ruimy, A.; Kergoat, L.; Bondeau, A.; Intercomparison, T.P.; Participants of The Potsdam NPP Model. Comparing global models of terrestrial net primary productivity (NPP): Analysis of differences in light absorption and light use efficiency. *Glob. Chang. Biol.* **1999**, *5*, 56–65. [[CrossRef](#)]
71. Clark, D.A.; Brown, S.; Kicklighter, D.W.; Chambers, J.Q.; Thomlinson, J.R.; Ni, J.; Holland, E.A. Errata: Net Primary Production in Tropical Forests: An Evaluation and Synthesis of Existing Field Data. *Ecol. Appl.* **2001**, *11*, 944. [[CrossRef](#)]
72. Martinez-Yrizar, A.; Sarukhan, J.; Perez-Jimenez, A.; Rincon, E.; Maass, J.M.; Solis-Magallanes, A.; Cervantes, L. Above-ground phytomass of a tropical deciduous forest on the coast of Jalisco, México. *J. Trop. Ecol.* **1992**, *8*, 87. [[CrossRef](#)]
73. Mackey, B.G.; Keith, H.; Berry, S.; Lindenmayer, D.B. *Green Carbon: The Role of Natural Forests in Carbon Storage. Part 1, A Green Carbon Account of Australia's South-Eastern Eucalypt Forest, and Policy Implications*; The Australian National University (ANU) Press: Canberra, Australia, 2008.
74. Cairns, M.A.; Olmsted, I.; Granados, J.; Argaez, J. Composition and aboveground tree biomass of a dry semi-evergreen forest on Mexico's Yucatan Peninsula. *For. Ecol. Manag.* **2003**, *186*, 125–132. [[CrossRef](#)]
75. Martinuzzi, S.; Gould, W.A.; Ramos Gonzalez, O.M.; Robles, A.M.; Maldonado, P.C.; Pérez-Buitrago, N.; Fumero Caban, J.J. Mapping tropical dry forest habitats integrating Landsat NDVI, Ikonos imagery, and topographic information in the Caribbean Island of Mona. *Rev. Biol. Trop.* **2008**, *56*, 625–639. [[CrossRef](#)] [[PubMed](#)]
76. Gonzalez, P.; Asner, G.P.; Battles, J.J.; Lefsky, M.A.; Waring, K.M.; Palace, M. Forest carbon densities and uncertainties from Lidar, QuickBird, and field measurements in California. *Remote Sens. Environ.* **2010**, *114*, 1561–1575. [[CrossRef](#)]
77. Castillo-Santiago, M.Á.; Ghilardi, A.; Oyama, K.; Hernández-Stefanoni, J.L.; Torres, I.; Flamenco-Sandoval, A.; Fernández, A.; Mas, J.-F. Estimating the spatial distribution of woody biomass suitable for charcoal making from remote sensing and geostatistics in central Mexico. *Energy Sustain. Dev.* **2013**, *17*, 177–188. [[CrossRef](#)]
78. Karl, J.W.; Maurer, B.A. Multivariate correlations between imagery and field measurements across scales: Comparing pixel aggregation and image segmentation. *Landsc. Ecol.* **2009**, *25*, 591–605. [[CrossRef](#)]
79. Hu, Q.; Wu, W.; Xia, T.; Yu, Q.; Yang, P.; Li, Z.; Song, Q. Exploring the Use of Google Earth Imagery and Object-Based Methods in Land Use/Cover Mapping. *Remote Sens.* **2013**, *5*, 6026–6042. [[CrossRef](#)]
80. Zolkos, S.G.; Goetz, S.J.; Dubayah, R. A meta-analysis of terrestrial aboveground biomass estimation using lidar remote sensing. *Remote Sens. Environ.* **2013**, *128*, 289–298. [[CrossRef](#)]
81. Hansen, M.C.; Potapov, P.V.; Moore, R.; Hancher, M.; Turubanova, S.A.; Tyukavina, A.; Thau, D.; Stehman, S.V.; Goetz, S.J.; Loveland, T.R.; et al. High-resolution global maps of 21st-century forest cover change. *Science* **2013**, *342*, 850–853. [[CrossRef](#)] [[PubMed](#)]

